LA-UR-13-20713
Approved for public release; distribution is unlimited.

Title: A molecular dynamics study of anisotropy and the effect of Xe on UO2 thermal conductivity

Author(s): Du, Shiyu
Gofryk, Krzysztof
Andersson, Anders D.
Liu, Xiang-Yang
Stanek, Christopher R.

Intended for: Report

A molecular dynamics study of anisotropy and the effect of Xe on UO_2 thermal conductivity

S. Du,[1] K. Gofryk,[1] D. A. Andersson,[1] X.-Y. Liu,[1] and C. R. Stanek[1]

[1] *Los Alamos National Laboratory, Los Alamos, New Mexico 87545 USA*

In this report we first investigate the effect of Xe on UO_2 thermal conductivity via molecular dynamics simulations. This property is studied both as function of temperature and for different concentrations and configurations of Xe atoms (randomly dispersed and in gas bubbles). The largest decrease of the thermal conductivity is obtained for randomly distributed Xe atoms, which is due to high defect scattering and thus decreasing phonon mean free path. Second we demonstrate several different manifestations of anisotropic UO_2 thermal conductivity, including discontinuities between the conductivity of bulk UO_2 separated by asymmetric grain boundaries and variations of the conductivity along different crystallographic directions in single crystals of UO_2. These results are validated against recent experiments on UO_2 single crystals.

INTRODUCTION

Thermal conductivity (κ) is an important material property in UO_2 nuclear fuel performance. It is a key parameter determining the temperature distribution and thus governing, e.g., dimensional changes due to thermal expansion, fission gas release rates and melting in accident scenarios. Therefore, accurate models of the variation of the thermal conductivity of UO_2 as a function of composition, microstructure and concentration of defects are crucial [1]. Furthermore, design of next generation nuclear fuels and understanding of accident scenarios stand to benefit from improved material models (including thermal conductivity) that rely less on empiricism and more on physics models capturing the state of the fuel, e.g. its composition and microstructure. Recently, atomistic simulations have been shown to be an effective tool for the calculation of UO_2 properties, including direct calculation of the thermal conductivity [2–4].

The first part of this report investigates the effect of fission gases (Xe) and their distribution in the lattice on UO_2 thermal conductivity, which is relevant for understanding the degradation of the thermal conductivity as function of burnup. The results are analyzed in terms of the Callaway model [14–16]. In previous studies we have reported Kapitza resistances of different UO_2 grain boundaries [12, 13]. A non-neglible difference was found between the Σ 5 tilt, Σ5 twist and random boundaries [13]. In addition, unexpected change in the temperature profiles along the heat flow direction was observed for asymmetric boundaries (e.g. the random grain boundary) when the molecular dynamics simulations were performed using sufficiently large simulations cells. This is not consistent with the expectation that the thermal conductivity of UO_2, crystallizing in the cubic fluorite structure, is isotropic. In the second part of this report the anisotropy of the UO_2 thermal conductivity is further explored. The results from the molecular dynamics simulations are also compared to recent experimental measurements of the thermal conductivity on oriented single crystals of UO_2.

METHODOLOGY

Molecular dynamics simulations applying the direct method, as described by Jund and Jullien [6], were used to calculate the thermal conductivity of UO_2. A constant heat flow is imposed in a rectangular prism simulation cell, i.e. an elongated box, by letting thermal energy transmit from a cold plate to a hot plate. The resulting temperature gradient is then monitored and averaged over time to obtain the thermal conductivity. The Basak potential [7] is used to calculate the inter-atomic forces between U and O atoms, while Geng's potential is used to account for interaction between Xe and other atoms [7]. The long-range electrostatic interaction was calculated by Wolf summation [8]. The length of simulation boxes range from 8 to 75 nm. The short cells suffer from fairly significant phonon scattering from the hot and cold plates. This is an artifact of the simulation setup, but the small cells are nevertheless useful for establishing physical trends. If the simulation cells contain defects or if the simulation temperature is high, the phonon mean free path may still be much shorter than the simulation cell and for such cases the results should be accurate. The longer simulations cells are used for extracting more precise values, which is especially important for pure UO_2 at low temperature. As much as possible we have attempted to perform simulations using similarly sized simulation boxes in order to maximize the cancellation of errors. The thickness of the hot and cold plates are 5.463 Å. The size of the time step is chosen to be 1.0 fs. The pre-equilibrium time is 250 ps and 500-1000 ps is used as the data acquisition time. All calculations were performed with the Scalable Parallel Short-range Molecular Dynamics (SPaSM) code [11].

RESULTS AND DISCUSSION

Effect of Xe on UO_2 thermal conductivity

Fission products and fission gases that accumulate as function of burnup significantly reduce the thermal conductivity of UO_2. This may occur due to point defect scattering by dispersed atomic defects or due to differences in the thermal conductivity between second phase precipitates, such as fission gas bubbles, and bulk UO_2. Xe is the most important fission gas and, consequently, it is interesting to examine the impact of dispersed Xe atoms in the UO_2 lattice and Xe atoms in fission gas bubbles on the thermal conductivity of this material. After annealing all fission gas atoms will more or less be present in bubbles since they are essentially insoluble in the lattice, however during irradiation a significant fraction is distributed within the UO_2 matrix as single atoms or small clusters. Calculations were performed for different concentrations of atomic defects and for microstructures where the fission gas atoms have precipitated into small bubbles.

Randomly dispersed Xe atoms

Analysis of the thermal conductivity (κ) carried by phonons relies on the following relation:

$$\kappa = \frac{1}{3} C v l \tag{1}$$

Here C is the heat capacity per volume, v is the average phonon velocity and l is the mean free path of phonons. The latter property is critical for understanding the degradation of the UO_2 thermal conductivity due to point defects (Xe atoms) and fission gas bubbles. Figure 1 shows the temperature dependence of the thermal conductivity for different concentrations of randomly dispersed Xe atoms. The calculations were performed for different simulation cells ranging from 26 to 75 nm in length. The length dependence is quite small, especially compared to pure UO_2, which can be explained by the fact that phonon scattering is dominated by Xe atoms acting as point scatterers rather than by artificial contributions from the hot and cold plates that may occur for short simulation cells of pure UO_2. Still the results from the 75 nm simulation cell should be considered to be the most reliable. Compared to pristine UO_2 (see Figure 4) Xe atoms decrease the thermal conductivity significantly, in particular at low temperature. The latter observation can qualitatively be explained by the fact that at high temperature there is significant phonon-phonon scattering due to anharmonicity and the corresponding phonon mean free path is short compared to the mean free path associated with Xe atoms acting as point scattering centers. At lower temperatures this relation is reversed.

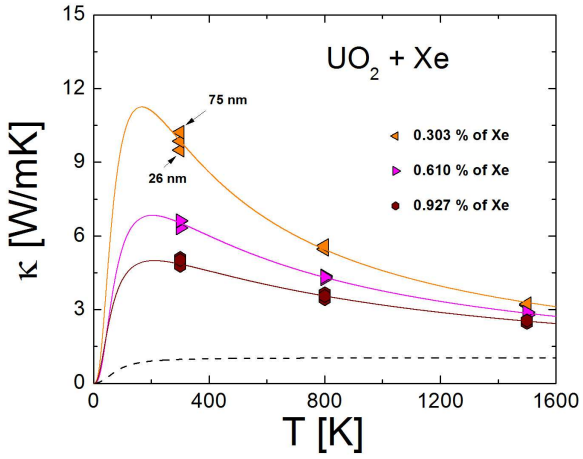

FIG. 1. The temperature dependence of the thermal conductivity of UO_2 for different concentration of Xe atoms. The solid lines are the Callaway model approximation and the dashed curve is minimal phonon thermal conductivity (see text).

In order to describe the temperature dependence of the thermal conductivity of UO_2 we use the Callaway model [14–16] to parameterize the relation in Eq. 1. The Callaway model relies on the Debye approximation for the phonon spectrum. The model takes into account different scattering mechanisms, such as point defects, boundaries and anharmonicity, in order to capture the temperature dependence of the thermal conductivity. In this approach the lattice thermal conductivity is written as:

$$\kappa_{\mathrm{L}}(T) = \frac{k_{\mathrm{B}}}{2\pi^2 \nu} \left(\frac{k_{\mathrm{B}} T}{\hbar}\right)^3 \int_0^{\Theta_{\mathrm{D}}/T} \frac{\tau_p x^4 e^x}{(e^x - 1)^2} dx \tag{2}$$

where ν is the velocity of sound, τ_{p} stands for the relaxation time (related to the mean free path in Eq. 1), $x = \hbar\omega/k_{\mathrm{B}}T$, ω is the phonon frequency, n is the number of atoms per unit volume, while $\hbar$, Θ_{D} and $\mathrm{k_B}$ are the reduced Planck constant, Debye temperature and the Boltzmann constant, respectively. In turn, the relaxation time in UO_2 may be accounted for by considering possible scattering mechanisms for the heat transport: point defect scattering, boundary scattering, and Umklapp processes, $\tau_{\mathrm{p}}^{-1} = \tau_{\mathrm{D}}^{-1} + \tau_{\mathrm{B}}^{-1} + \tau_{\mathrm{U}}^{-1}$, where the particular inverse relaxation times are given by the following expressions:

$$\begin{aligned} \tau_{\mathrm{D}}^{-1} &= D x^4 T^4, \\ \tau_{\mathrm{B}}^{-1} &= B, \\ \tau_{\mathrm{U}}^{-1} &= U T^3 x^2 e^{\frac{-\Theta_{\mathrm{D}}}{2T}} \end{aligned} \tag{3}$$

Taking the sound velocity $\nu = 2965$ m/s, as calculated from $\nu = k_B \Theta_{\mathrm{D}}/\hbar \sqrt[3]{6\pi^2 n}$ and n being the number of atoms per unit volume, the experimental or calculated

$\kappa_L(T)$ variation can be well fitted by Eq. 2, as shown by the lines in Figure 1. The relative weight parameters for the different phonon scattering processes obtained from this fit are summarized in Table I. As expected, increasing the concentration of Xe atoms results in increase of the scattering rate by defects. There is a rough correlation between this parameter and the average separation between Xe atoms, which is supposedly governing the effective mean free path. Further analysis will be performed in order to determine whether this relation can be quantified. The point defect scattering rate is much larger than for pure UO_2, which is also an expected result. The simulation cells do not contain any boundaries so, in principle, the boundary contribution should be zero. However, it is expected that boundary-like scattering occurs from the hot and cold plates or due to the periodic boundary conditions of the simulation cells. Even for the long simulation cells applied here the effect of the hot and cold plates is not completely eliminated. The Umklapp scattering parameter (phonon-phonon scattering due to anharmonicity) is approximately independent of the Xe concentration, while it is slightly larger than for pure UO_2 (averaged over the crystallographic directions).

It is interesting to compare the calculated lattice thermal conductivity of UO_2 with the theoretically achievable minimal magnitude of the phonon contribution. The latter may be calculated from the expression [17, 18]:

$$\kappa_{L_{min}}(T) = \left(\frac{3n}{4\pi}\right)^{1/3} \frac{k_B^2 T^2}{\hbar\theta_D} \int_0^{\Theta_D/T} \frac{x^3 e^x}{(e^x-1)^2} dx \quad (4)$$

Here no distinction is made between the transverse and longitudinal acoustic phonon modes. The result obtained for UO_2 with randomly distributed Xe atoms ($\Theta_D = 370$ K and $n = 7.3 \times 10^{28}$ m^{-3}) is shown in Fig. 1 by the dashed line. Apparently, $\kappa_{L_{min}}$ is much smaller than the calculated κ_L in the entire temperature range. In strongly atomically disordered materials the mean free path of phonons is short because of scattering by atomic disorder. In such materials the lattice thermal conductivity measured at high temperatures approach nearly $\kappa_{L_{min}}$. In general, the boundary scattering is dominant at low temperatures, while the phonon Umklapp scattering is important at high temperatures. Besides these two mechanisms the position of the maximum in $\kappa(T)$ and its characteristic shape is mainly governed by point defect scattering (point defects are always existing in "real" materials).

Fission gas bubbles and interaction with grain boundaries

In order to evaluate the effect of different configurations of Xe atoms in the UO_2 lattice (including interaction with grain boundaries), calculations on five types of structures were performed at 300 K in the 25 nm simulation box. Type I: structures with one Xe bubble but no grain boundary; Type II: structures with a grain boundary but no Xe atoms; Type III: structures with a grain boundary and randomly distributed Xe atoms corresponding to the Xe concentration for one (1b) or three (3b) bubbles, Type IV: structures with one Xe gas bubble on the grain boundary; and Type V: structures with either one (1b) or three (3b) Xe gas bubbles near the grain boundary. An example of the simulation setup is shown in Figure 2. In this work we refer to the configuration in which Xe bubbles are positioned in the bulk part between the two grain boundaries as "near the boundary" since the distance between the bubble to each boundary is short. All the results, including the reference structure with neither Xe atoms nor any grain boundary, are shown in Figure 3. As expected we find that both Xe and grain boundaries lower the thermal conductivity. This is consistent with our previous calculations of the Kapitza resistance of grain boundaries [13]. It is also clear that randomly distributed fission gas atoms (Type III) lower the thermal conductivity more than Xe atoms in fission gas bubbles (Type IV and V). This is because randomly distributed Xe atoms change the heat transfer throughout the crystal structure by decreasing the phonon mean free path, while the other types of structures mainly have local effects near the gas bubbles or boundaries. The separation between bubbles is much larger than between the individual Xe atoms in the randomly dispersed system, which explains the more significant impact on the phonon mean free path in the former case. Comparing the Type IV and V structures, the effective thermal conductivity decreases more when the fission gas bubble is located at the boundary than away from the boundary or in the bulk. Additional data is required to perform a quantitative analysis of these effects.

The role of temperature on structures with fission gas

TABLE I. Scattering parameters for the thermal conductivity of UO_2 single crystal for three different crystallographic directions (see text) derived from the Callaway approach (UO_2). The same data for the thermal conductivity of UO_2 single crystals containing three different concentrations of randomly dispersed Xe (UO_2 with Xe).

	D [K^{-4}s^{-1}]	B [s^{-1}]	U [K^{-3}s^{-1}]
UO_2			
$\Delta T\|\|100$, 30 nm	6.0×10^2	4.9×10^{11}	2.87×10^5
$\Delta T\|\|110$, 30 nm	5.9×10^2	4.8×10^{11}	2.49×10^5
$\Delta T\|\|111$, 30 nm	5.7×10^2	4.6×10^{11}	2.45×10^5
UO_2 with Xe			
Xe, 0.303 %	1.1×10^3	4.1×10^{11}	2.95×10^5
Xe, 0.610 %	1.3×10^3	3.7×10^{11}	2.9×10^5
Xe, 0.927 %	3.9×10^3	2.4×10^{11}	2.86×10^5

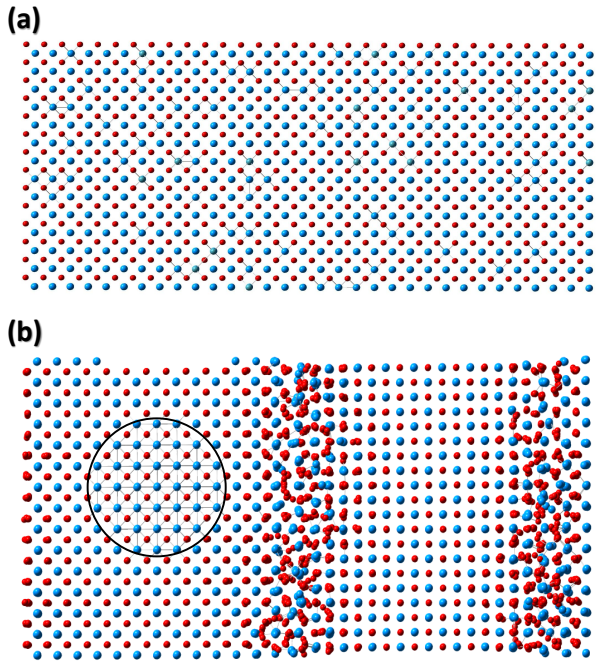

FIG. 2. The structures of the 8 nm x 3.8 nm x 3.8 nm UO_2 simulation cells with (a) randomly distributed Xe atoms and (b) with bubble near the grain boundary (see text).

and a grain boundaries has also been considered. The 25 nm × 3.8 nm × 3.8 nm simulation box was used to perform simulations at 300 K, 800 K and 1500 K. The results are shown in Figure 3. Type III structures have the lowest thermal conductivity for the whole temperature range. For this case the temperature dependence is rather weak, which can be explained by the fact that since the phonon mean free path is already short due to point defect scattering the phonon-phonon scattering occurring at high temperature has much smaller impact. Conversely, for other cases where the mean free path is not as severely limited by the presence of point defect scatterers the temperature dependence is much stronger. The difference between the structures decreases at high temperature. This is related to the phonon-phonon scattering due to anharmonicity eventually controlling the phonon mean free path for all structures at high temperature. Up to the maximum simulation temperature (1500 K) Type III structures still have significantly lower thermal conductivity than any others.

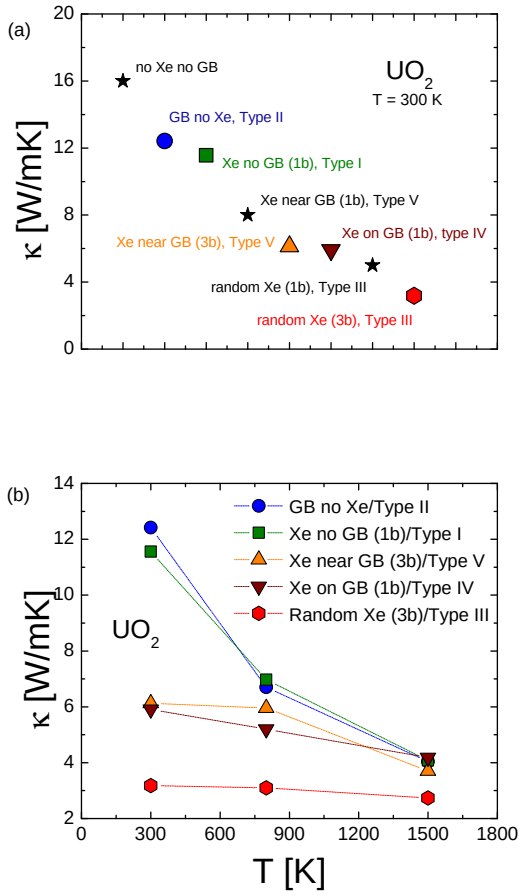

FIG. 3. (a) The thermal conductivity of UO_2 with different defect structures (GB stands for grain boundary, random for randomly distributed Xe atoms). The Type designation corresponds to the notation introduced in the text. Type I: structures with one Xe bubble but no grain boundary; Type II: structures with a grain boundary but no Xe atoms; Type III: structures with a grain boundary and randomly distributed Xe atoms corresponding to the Xe concentration for one (1b) or three (3b) bubbles, Type IV: structures with one Xe gas bubble on the grain boundary; and Type V: structures with either one (1b) or three (3b) Xe gas bubbles near the grain boundary. The thermal conductivity values were calculated at 300 K with a simulation box of length 25 nm. (b) Thermal conductivity of UO_2 calculated for different defect structures at 300 K, 800 K and 1500 K (see text).

Anisotropic UO_2 thermal conductivity

Calculation of the Kapitza resistance of grain boundaries relies on the bulk thermal conductivity on each side of the boundary being the same [10]. In materials with cubic crystal structure the thermal conductivity is assumed to be isotropic, i.e. the thermal conductivity tenser κ_{ij} fulfills $\kappa_{ii} \neq 0$ and $\kappa_{ij} = 0$. Since UO_2 crystallizes in the cubic fluorite structure, the thermal conductivity is expected to be isotropic and we have not been able to find any reports of non-diagonal terms in the UO_2 thermal conductivity tensor. Contrary to this assumption, calculation of the Kapitza resistance for the random grain boundary showed different temperature profiles on the two sides of the boundary. This only occurred when the length of the simulation cell exceeded a critical value. Below this length the scattering from the hot and cold

plates likely masked the effect. The effect is not present in any of symmetric grain boundary simulations, where the temperature gradient is along the same crystallographic direction on both sides of the grain boundary. For the random boundary the temperature gradient is along the 100 direction on one side and along the 110 direction on the other side. These results suggest that the unexpected result for the random boundary is related to anisotropy of the UO_2 thermal conductivity, despite its cubic fluorite crystal structure.

In order to test this hypothesis we performed simulations for bulk UO_2 with the temperature gradient along the principal 100, 110 and 111 crystallographic directions. The results are show in Figure 4 for the 30 nm simulation cell. The lowest thermal conductivity is obtained in the 100 direction, followed by 110 and 111 (highest). For the 30 nm simulation cell the difference is approximately 20% between the minimum and the maximum conductivity at 300 K. This difference persists even at high temperature, which is somewhat surprising since the increased anharmonicity could be expected to wash out these differences. The sensitivity of this conclusion with respect to the length of the simulation cell was investigated at 300 K. The inset of Figure 4 shows that the anisotropy is even higher for short simulation cells and extrapolating the results beyond the largest simulation cell of 60 nm indicates that it should remain even at infinite length. For the largest simulation cell at 300 K, the thermal conductivity in the 111 direction is about 9% higher than in the 100 direction.

In order to validate our predictions we are currently performing experiments on UO_2 single crystals. The initial results confirm the predictions from molecular dynamics simulations, at least up to room temperature. At 300 K the experimental thermal conductivity is 7.56 W/mK and 8.8 W/mK for the 100 and 110 directions, respectively. Even though the absolute thermal conductivities differ between theory and simulations (a well-known deficiency of the empirical potentials), the relative difference between the 100 and 110 directions are similar (13 % in experiments and 16% in experiments). Experiments are under way for the 111 direction.

We have also performed calculations of the thermal conductivity along the principal crystallographic lattice directions for cells with different concentrations of randomly dispersed Xe atoms. These results are shown in Figure 5. The difference in the thermal conductivity along the crystallographic directions is suppressed and overall the magnitude of the thermal conductivity is significantly lowered when Xe atoms are embedded into the crystals, which agrees with the previous conclusions.

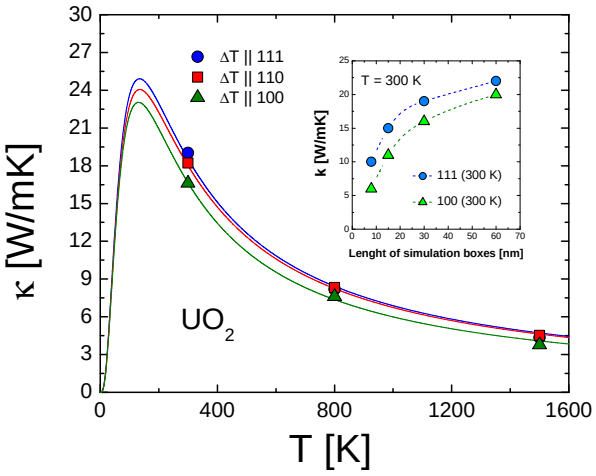

FIG. 4. The thermal conductivity of UO_2 single crystals calculated for the 100, 110 and 111 crystallographic directions. The lines are guide for the eye. The inset shows the thermal conductivity vs. the length of simulation boxes obtained at 300 K for the 100 and 111 crystallographic directions.

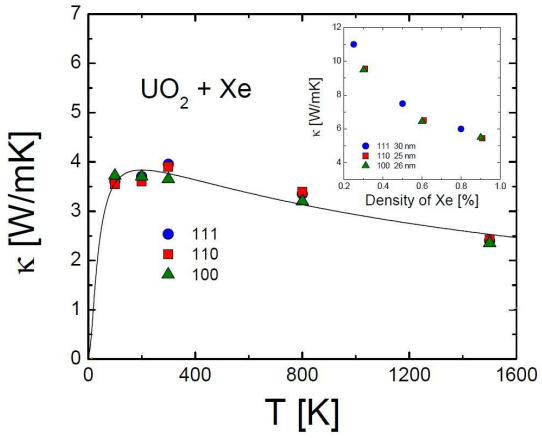

FIG. 5. The thermal conductivity of UO_2 single crystals containing randomly dispersed Xe atoms calculated for 100, 110 and 111 crystallographic directions in the 8 nm × 3.8 nm × 3.8 nm cell. The lines are guide for the eye. The inset shows the thermal conductivity vs. Xe concentration at 300 K and for the 100, 110 and 111 crystallographic directions.

SUMMARY AND CONCLUSIONS

The presence of Xe atoms decreases the thermal conductivity of UO_2, with the largest effect occurring for randomly dispersed Xe atoms acting as point scatterers. Fission gas bubbles have a smaller effect. At high temperature phonon scattering is dominated by anharmonicity and the impact of the distribution of fission gas atoms is less drastic. Simulations of the temperature profiles across asymmetrical grain boundaries revealed that

UO_2 has asymmetric thermal conductivity, i.e. non-zero off-diagonal terms in the conductivity tensor. For cubic materials such as fluorite UO_2 this is a highly unexpected result. These findings were confirmed by performing simulations for bulk UO_2 along the principal crystallographic directions. The lowest conductivity was obtained along the 100 direction and the highest along the 111 direction, with a difference of 10-20 % which prevails even at high temperature. These findings were confirmed for the 100 and 110 directions by recent experiments on UO_2 single crystals up to 300 K.

[1] P.J. Lucuta, Hj. Matzka and I.J. Hastings, J. Nucl. Mater. **232**, 166 (1996).

[2] T. Watanabe, S. G. Srivilliputhur, P. K. Schelling, J. S. Tulenko, S. B. Sinnott and S. R. Phillpot, J. Am. Ceram. Soc. **92**, 850 (2009).

[3] D. A. Vega, T. Watanabe, S. B. Sinnott, S. R. Phillpot, J. S. Tulenko, Nucl. Tech. **165**, 308 (2009).

[4] S. R. Phillpot, A. El-Azab, A. Chernatynskiy and J. S. Tulenko, JoM **63**, 73 (2011).

[6] P. Jund and R. Jullien, Phys. Rev. B **59**, 13707 (1999).

[7] C. B. Basak, A. K. Sengupta and H. S. Kamath, J. Alloys Compd. **360**, 210 (2003).

[7] H. Y. Geng, Y. Chen, Y. Kaneta and M. Kinoshita, J. Alloys Compd. **457**, 465 (2008).

[8] D. Wolf, P. Keblinski, S. R. Phillpot and J. Eggebrecht, J. Chem. Phys. **110**, 8254 (1999).

[9] P. L. Kapitza, J. Phys.-USSR **4**, 181 (1941).

[10] H.-S. Yang, G.-R. Bai, L. J. Thompson and J. A. Eastman, Acta Mater. **50**, 2309 (2002).

[11] K. Kadau, T. C. Germann and P. S. Lomdahl, Int. J. Mod. Phys. C **17**, 1755 (2006).

[12] P. V. Nerikar, K. Rudman, T. G. Desai, D. Byler, C. Unal, K. J. McClellan, S. R. Phillpot, S. B. Sinnott, P. Peralta, B. P. Uberuaga and C. R. Stanek, J. Am. Ceram. Soc. **94**, 1893 (2011).

[13] M. Tonks et al., submitted.

[14] J. Callaway, Phys. Rev. **113**, 1046 (1959).

[15] J. Callaway and H. C. von Baeyer, Phys. Rev. **120**, 1149 (1960).

[16] J. Callaway, Phys. Rev. **122**, 787 (1961).

[17] K. Gianno, A. V. Sologubenko, M. A. Chernikov, H. R. Ott, I. R. Fisher and P. C. Canfield, Phys. Rev. B **62**, 292 (2000).

[18] D. G. Cahill, R. O. Pohl, Solid State Commun. **70**, 927 (1989).